

INFORMATION TO USERS

The most advanced technology has been used to photograph and reproduce this manuscript from the microfilm master. UMI films the original text directly from the copy submitted. Thus, some dissertation copies are in typewriter face, while others may be from a computer printer.

In the unlikely event that the author did not send UMI a complete manuscript and there are missing pages, these will be noted. Also, if unauthorized copyrighted material had to be removed, a note will indicate the deletion.

Oversize materials (e.g., maps, drawings, charts) are reproduced by sectioning the original, beginning at the upper left-hand corner and continuing from left to right in equal sections with small overlaps. Each oversize page is available as one exposure on a standard 35 mm slide or as a 17" × 23" black and white photographic print for an additional charge.

Photographs included in the original manuscript have been reproduced xerographically in this copy. 35 mm slides or 6" × 9" black and white photographic prints are available for any photographs or illustrations appearing in this copy for an additional charge. Contact UMI directly to order.



300 North Zeeb Road, Ann Arbor, MI 48106-1346 USA

PREVIEW

Order Number 8818617

**Electronic structure of rare earth magnets and tungsten-based
transition metal alloys by photoelectron spectroscopy**

Engelhardt, Michael Anthony, Ph.D.

The University of Nebraska - Lincoln, 1988

U·M·I
300 N. Zeeb Rd.
Ann Arbor, MI 48106

PREVIEW

**ELECTRONIC STRUCTURE OF RARE EARTH MAGNETS
AND TUNGSTEN-BASED TRANSITION METAL ALLOYS
BY PHOTOELECTRON SPECTROSCOPY**

by

Michael A. Engelhardt

A DISSERTATION

**Presented to the Faculty of
The Graduate College in the University of Nebraska
In Partial Fulfillment of Requirements
For the Degree of Doctor of Philosophy**

Major: Physics and Astronomy

Under the Supervision of Professor David J. Sellmyer

Lincoln, Nebraska

May 1988

TITLE

Electronic Structure of Rare Earth Magnets and
Tungsten-Based Transition Metal Alloys by Photoelectron Spectroscopy

BY

Michael A. Engelhardt

APPROVED

DATE

<u>Prof. David J. Sellmyer</u>	<u>April 25, 1988</u>
<u>Prof. Roger D. Kirby</u>	<u>April 25, 1988</u>
<u>Prof. Sitaram S. Jaswal</u>	<u>April 25, 1988</u>
<u>Prof. John A. Woollam</u>	<u>April 25, 1988</u>
<u> </u>	<u> </u>
<u> </u>	<u> </u>
<u> </u>	<u> </u>

SUPERVISORY COMMITTEE

GRADUATE COLLEGE

UNIVERSITY OF NEBRASKA

ELECTRONIC STRUCTURE OF RARE EARTH MAGNETS
AND TUNGSTEN-BASED TRANSITION METAL ALLOYS
BY PHOTOELECTRON SPECTROSCOPY

Michael A. Engelhardt, Ph.D.

University of Nebraska, 1988

Adviser: David J. Sellmyer

Photoelectron spectroscopy was used to investigate the electronic and magnetic structures of crystalline rare earth magnetic materials of the form $R_2Fe_{14}B$ with $R = Y, Nd, \text{ and } Gd$. Measurements are reported for photon energies of 21.2 eV, 40.8 eV, 100 eV and 130 eV. The major features of the spectra include an Fe(3d) band centered at $E_B = -0.7$ eV, Gd(4f) at -8.8 eV, Nd(4f) at -5.3 eV, and B(2s) at -8.6 eV. These results compare favorably with self-consistent, semi-relativistic, spin-polarized linear-muffin-tin-orbital calculations of Jaswal for $Y_2Fe_{14}B$. Measurements were made in both the ferromagnetic state ($T = 296$ K) and paramagnetic state ($T = 623$ K). No change in the photoelectron intensity was detected on heating above the Curie point $T_C = 585$ K. This constancy of the electronic density of states indicates a paramagnetic state with considerable magnetic short-range order, as in the fluctuating band model of itinerant ferromagnetism.

In addition, binary transition metal alloys of the form T_xW_{100-x} where $T = Cu, Ni, \text{ and } Co$ are investigated by photoelectron spectroscopy, x-ray diffraction, and x-ray fluorescence. For each series, seven to nine x compositions were produced by sputtering. X-ray

diffraction measurements show amorphous phases occurring from $52 < x < 65$ for $\text{Cu}_x\text{W}_{100-x}$, $30 < x < 50$ for $\text{Ni}_x\text{W}_{100-x}$, and $15 < x < 80$ for $\text{Co}_x\text{W}_{100-x}$. Photoelectron spectra are presented for photon energies of 21.2 eV and 40.8 eV. Spectra for the CuW series show that the Cu d-band peak ($E_B = -2.2$ eV) in pure Cu shifts to $E_B = -2.9$ eV upon alloying to $\text{Cu}_{81}\text{W}_{19}$. Measurements for the NiW and CoW series exhibit a smaller d-band peak shift of approximately 0.3 eV away from e_F as the composition changes to pure tungsten. The alloys appear to fit the split-band model which is described with the coherent potential approximation.

ACKNOWLEDGEMENTS

I would like to thank my advisor David Sellmyer for his guidance and support. I feel fortunate to have been one of his students.

For their assistance with computer and electronic systems within the lab, I am indebted to David Billesbach and Roger Kirby. I would also like to thank J. A. R. Samson for his technical support in designing the discharge lamp and for explanations of the electron analyzer. Thanks go to Kevin Aylesworth and Yong-Gang Ren for their assistance in performing x-ray diffraction and x-ray fluorescence measurements. Also, thanks to John Bob Kelty, Don Fuehring and the shops for their guidance in designing electronic and mechanical components. In addition, David Liebowitz must be acknowledged for his work on the initial set-up of the photo-emission laboratory.

I am grateful for contributions to this dissertation by my wife Cathy. Her expertise and support were valuable in the lab and her wordprocessor skills contributed to the completion of this project.

Finally, I would like to thank the Department of Energy, the National Science Foundation, Dale Electronics, and the Alcoa Corporation for financial support.

TABLE OF CONTENTS

List of Figures	i
List of Tables	iii
 1. Photoelectron Spectroscopy	 1
1.1 Theory	1
1.2 PES of Rare Earth Magnetic Materials	8
1.3 PES of Intertransition-Metal Alloys	9
 2. Experimental Methods	 12
2.1 Vacuum System	12
2.2 UHV Chamber Arrangement	14
2.3 Helium Discharge Lamp	16
2.4 Sample Manipulator	21
2.5 Cylindrical Mirror Analyzer	21
2.6 Electron Multiplier	33
2.7 Sputtering	33
2.8 Experimental Procedures	38
2.9 Data Collection and Analysis	39
 3. The $R_2Fe_{14}B$ Alloys	
3.1 Introduction	43
3.2 Sample Preparation	43
3.3 Photoelectron Spectroscopy Measurements.	44
3.4 Conclusion	53

4 . The TW Alloys	
4.1 Introduction	54
4.2 Sample Preparation	54
4.3 Characterization	
4.3.1 X-Ray Fluorescence	60
4.3.2 X-Ray Diffraction	66
4.4 Photoelectron Spectroscopy Measurements.	71
4.5 Conclusion	87
References	88

PREVIEW

LIST OF FIGURES

1. Schematic diagram of photoelectric effect	3
2. Mean free path of electrons in solids	5
3. Crystal structure of $\text{Nd}_2\text{Fe}_{14}\text{B}$	10
4. Experimental vacuum system	13
5. Schematic diagram of UHV components	15
6. Schematic diagram of positions of UHV components for alignment	17
7. Discharge lamp	18
8. Discharge lamp and differential pumping assembly	19
9. Sample holder	22
10. Diagram of cylindrical mirror analyzer	24
11. Cylindrical mirror assembly	25
12. Experimental work function	30
13. Schematic of angular uncertainties	32
14. Detector electronics	34
15. Quadropole mass spectrum	36
16. Sputtering gun beam profile	37
17. Data collection electronics	40
18. Block diagram of data collection program	42
19. He I and He II spectra for the $\text{R}_2\text{Fe}_{14}\text{B}$ compounds	45
20. Photoelectron spectra for $\text{Nd}_2\text{Fe}_{14}\text{B}$ near and off the 4d-4f resonance of Nd	48
21. He I spectra for $\text{Nd}_2\text{Fe}_{14}\text{B}$ in the paramagnetic state	49

22. Spin-polarized densities-of-states	51
23. Comparison of $\text{Nd}_2\text{Fe}_{14}\text{B}$ PES spectrum with $\text{Y}_2\text{Fe}_{14}\text{B}$ calculation	52
24. Sputtering machine	56
25. Sputtering rate calibration	65
26. X-ray diffraction of $\text{Cu}_x\text{W}_{100-x}$ with $x=43$ to 100	67
27. X-ray diffraction of $\text{Cu}_x\text{W}_{100-x}$ with $x=0$ to 43	68
28. X-ray diffraction of $\text{Ni}_x\text{W}_{100-x}$	69
29. X-ray diffraction of $\text{Co}_x\text{W}_{100-x}$	70
30. He I PES spectra for $\text{Cu}_x\text{W}_{100-x}$	73
31. He II PES spectra for $\text{Cu}_x\text{W}_{100-x}$	74
32. He I PES spectra for $\text{Ni}_x\text{W}_{100-x}$	75
33. He II PES spectra for $\text{Ni}_x\text{W}_{100-x}$	76
34. He I PES spectra for $\text{Co}_x\text{W}_{100-x}$	77
35. He II PES spectra for $\text{Co}_x\text{W}_{100-x}$	78
36. Peak shifts for CuW	84
37. Peak shifts for NiW	85
38. Peak shifts for CoW	86

LIST OF TABLES

1. Cylindrical mirror analyzer dimensions	23
2. Compositional analysis of $\text{Cu}_x\text{W}_{100-x}$	61
3. Compositional analysis of $\text{Ni}_x\text{W}_{100-x}$	62
4. Compositional analysis of $\text{Co}_x\text{W}_{100-x}$	63
5. Spectral intensities	79
6. Peak positions for $\text{Cu}_x\text{W}_{100-x}$	81
7. Peak positions for $\text{Ni}_x\text{W}_{100-x}$	82
8. Peak positions for $\text{Co}_x\text{W}_{100-x}$	83

CHAPTER 1

PHOTOELECTRON SPECTROSCOPY

Photoelectron spectroscopy (PES) makes use of the photoelectric effect which was first observed experimentally by Hertz¹ in 1887 and was subsequently described by Einstein² in 1905. In a solid, the absorption of radiation results in photoelectrons -- electrons which are liberated from the solid. The photoelectric effect has developed into a sophisticated spectroscopic technique for the study of metals. The physical and chemical properties of metals are inherently related to the electronic structure, particularly the valence electronic states. PES measurements provide insight into the microscopic properties which are the basis for macroscopic properties such as magnetic behavior, superconductivity and specific heat³.

1.1 THEORY

Electrons in a metal can absorb light with photon energy $h\nu$ and be excited to higher energy levels. Given sufficient energy the electrons are transported to the surface and escape from the metal. The maximum kinetic energy of such an electron is

$$E_{\max} = h\nu - e\phi$$

where $e\phi$ is the work function. By analyzing the energies of photoelectrons, the electronic states may be studied⁴. At low photon energies (which exceed the workfunction), valence electrons are ejected.

At higher photon energies, the electrons from core levels may also be emitted.

The photoemission process is summarized by Berglund and Spicer⁵ into what is known as the three-step model. The model includes:

- 1) photoexcitation of an electron
- 2) the transport of the electron to the surface
- 3) the electron leaving the bulk.

The emitted electrons form an emission spectrum where the intensity is related to the electronic density of states (DOS). The emission spectrum is called the energy distribution curve (EDC). Figure 1 shows a schematic diagram of the photoelectric effect and the resulting photoelectron distribution.

The emission intensity is a convolution of both the availability of an initial state electron and a final state. Variations in the availability of continuum states interfere with easy interpretation of the occupation of the initial states. These variations can exist for electrons leaving the surface at low energies near the vacuum level. For photon energies above 20 eV, valence band photoelectrons are for the most part free of these final state effects⁶.

The density of states $N(E)$ is defined by Margaritondo and Weaver as⁷

$$N(E) \propto \int_{\mathbf{k} \text{ space}} \frac{dS_{\mathbf{k}}}{|\nabla_{\mathbf{k}} E_i(\mathbf{k})|}$$

where $S_{\mathbf{k}}$ defines a constant energy surface and E_i is the initial elec-

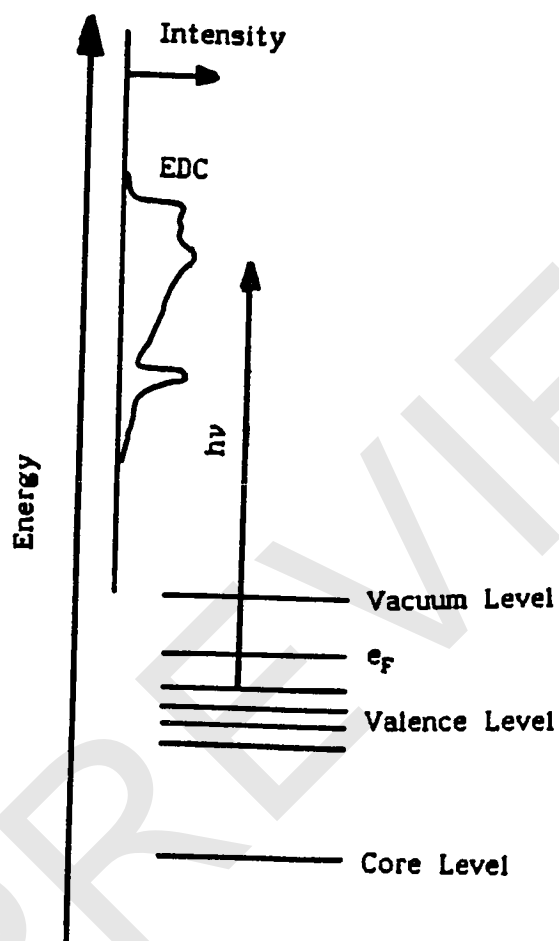


Fig. 1. Schematic diagram of the energy levels in a metal undergoing photoelectron emission.

tronic state. What must be determined is how the DOS is reflected in the photoelectron spectrum (EDC).

The EDC may be broken into two portions⁶: the intensity $I_p(E, h\nu)$ of primary electrons which have not lost any energy in scattering and the intensity $I_s(E, h\nu)$ of secondary electrons which are inelastically scattered. The measured EDC intensity $I(E, h\nu)$ is then

$$I(E, h\nu) = I_p(E, h\nu) + I_s(E, h\nu)$$

Using the three-step model, the energy distribution of primary electrons is given by⁶

$$I_p(E, h\nu) = P(E, h\nu) T(E) D(E)$$

Here, $P(E, h\nu)$ is the distribution of photoexcited electrons, $T(E)$ is the transport term which models the movement of the electron after the photoexcitation, and $D(E)$ is the surface transition term for escape from the surface. The terms $T(E)$ and $D(E)$ are slowly varying with energy; therefore, they do not contribute to structure in the EDC. Their effect is limited to modulating the relative intensities of spectral features.

Electrons which are inelastically scattered in the solid may or may not reach the surface and escape. The escape probability is influenced by the energy-dependent electron mean free path⁷ shown schematically in Fig. 2. Those secondary electrons which escape and are detected will have smaller kinetic energies than the elastically scattered primary electrons. They contribute to a broad low-energy peak in the EDC.

The distribution of photoexcited electrons $P(E, h\nu)$ can be calcu-

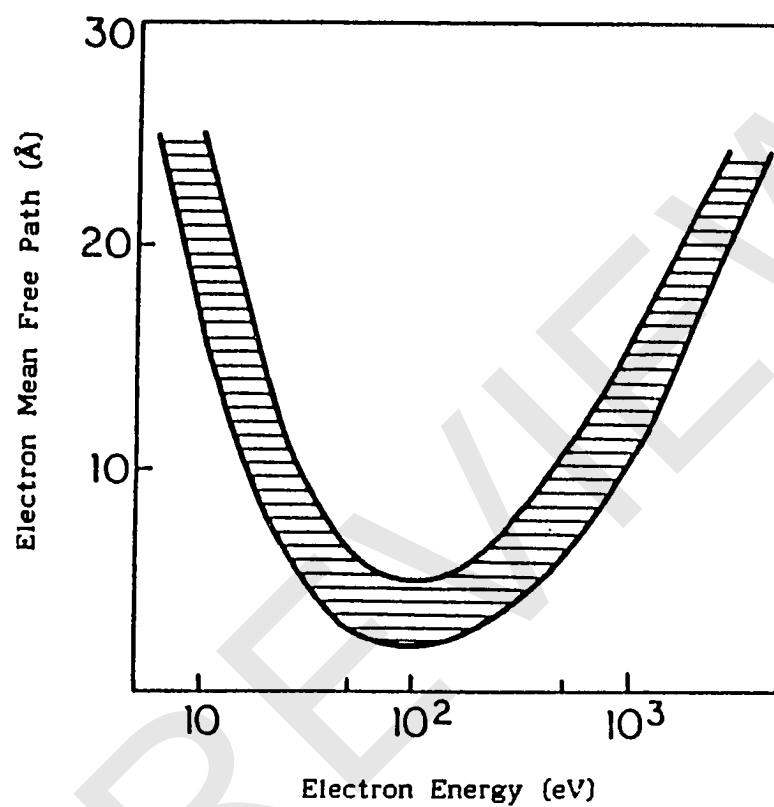


Fig. 2. Mean free path of electrons in solids. Taken from Ref. 7.

lated by considering the photoabsorption process from the occupied states E_i into the empty states E_f . Here, the initial state and the final state are separated by the photon energy $h\nu$:

$$E_f(\vec{k}) - E_i(\vec{k}) = h\nu$$

Additionally, the final state must correspond to the kinetic energy selected by the analyzer⁸

$$E_f(\vec{k}) - e\phi = E$$

The distribution of photoexcited electrons is then

$$P(E, h\nu) \propto \sum_{i,f} \int d^3k \left| \langle f | \nabla | i \rangle \right|^2 \delta [E_f(\vec{k}) - E_i(\vec{k}) - h\nu] \times \delta [E_f(\vec{k}) - E]$$

The optical transition probability between the initial and final states is given by the Fermi golden rule

$$P_{if} \propto \left| \langle f | \nabla | i \rangle \right|^2$$

To calculate P_{if} , the initial $|i\rangle$ and final $\langle f|$ state wavefunctions must be known. Because of the difficulty in calculating these quantities, an approximation is made by considering this term constant. Failures of this approximation are indicated by the extent to which the spectral features of the EDC's change with photon energy⁹. By using different photon energies, the electrons may be excited into different final states.

Taking the matrix element as a constant, we arrive at the energy distribution of the joint density of states (EDJDOS)

$$P(E, h\nu) \propto \sum_{i,f} \int d^3k \delta[E_f(\vec{k}) - E_i(\vec{k}) - h\nu] \times \delta[E_f(\vec{k}) - E]$$

The delta functions define two surfaces in k space and their intercept defines a line L in k space⁷. The integral may be rewritten as a line integral

$$P(E, h\nu) \propto \int_{k \text{ space}} \frac{dL_k}{|\nabla_k E_f(\vec{k}) \times \nabla_k E_i(\vec{k})|}$$

which is similar to the expression obtained for the DOS $N(E)$.

The photoelectron spectrum is not an exact replica of the EDJDOS due to contributions from the optical transition probability term, the slowly varying transport and surface terms, and the background of scattered electrons. For the photon energies of interest in this dissertation, the modulation of the EDC by the final state is negligible. PES spectra are interpreted as reflecting the features of the initial state with a scattered electron background.

Studies of the valence electrons aid in understanding the bulk properties of metals, their alloys and compounds. The behavior of these electrons is characterized and modeled by comparisons of PES measurements and electronic structure calculations. This enables the development of predictive models.

1.2 PES OF RARE EARTH MAGNETIC MATERIALS

The rare earth materials are of interest because of their uses in the leading edge technologies of permanent magnets and magneto-optic information storage systems. In addition to having a valence band (from 5d and 6s states), they have 4f levels which are near the fermi edge and are therefore accessible to PES measurements¹⁰. The 4f band is filled as the rare earth series develops from La to Lu. This partly filled 4f shell is the source of many of the properties of the rare earth elements.

These materials also show interesting behavior in terms of their valence states which may be nonintegral in valence and vary with specific environments. Studies of rare earth materials with Ce have been done¹¹ and show that Ce may have a valence of +3 or an intermediate valence less than +3.

PES measurements have been carried out on only a few rare earth materials since they are reactive and oxidize readily. The valence bands and 4f levels for pure metals have been measured¹² to 20 eV on either side of the fermi edge by XPS (x-ray photoelectron spectroscopy) and BIS (bremsstrahlung isochromat spectroscopy). Two comprehensive reviews of rare earth materials have been compiled; the first by Campagna, Wertheim, and Baer¹³ which covers PES measurements of the compounds of rare earth metals with rare earth borides, antimonides, chalcogenides, pnictides, halides, and intermetallics. The second review, by Netzer and Matthew¹⁴, investigates the surfaces of rare earth metals by a variety of surface techniques. Additional studies

have been conducted on rare earth glasses. Examples of rare earth glass measurements include an XPS study of Gd-Co and Gd-Fe amorphous films¹⁵ and UPS (ultraviolet photoelectron spectroscopy) and XPS studies of Gd₂Co and Er₂Co glasses¹⁶.

The rare earth permanent magnet material Nd₂Fe₁₄B has opened new vistas for the use of permanent magnets¹⁷. With an energy product as high as 50 MgOe, this material can be used to improve existing magnetic devices and create new ones¹⁸. Investigation of the microscopic structure of Nd₂Fe₁₄B by PES gives insight into its extraordinary magnetic properties.

The structure of the magnetic material consists of a 68 atom unit cell¹⁹. The structure is tetragonal P4₂/mm as shown in Fig. 3. The unique arrangement of the atoms provides structural stability and places the moment-bearing atoms in positions that allow for previously unattainable magnetic properties.

In Chapter 3, results are presented of photoemission measurements on crystalline R₂Fe₁₄B alloys, where R = Y, Nd, and Gd. These measurements help lead to a predictive model for the magnetic behavior and electronic structure of these materials by comparison with band calculations.

1.3 PES OF INTERTRANSITION-METAL ALLOYS

Work with transition metal binary alloys has proceeded with the desire to understand the mechanisms of their physical and electronic properties such as how they form amorphous or crystalline phases.

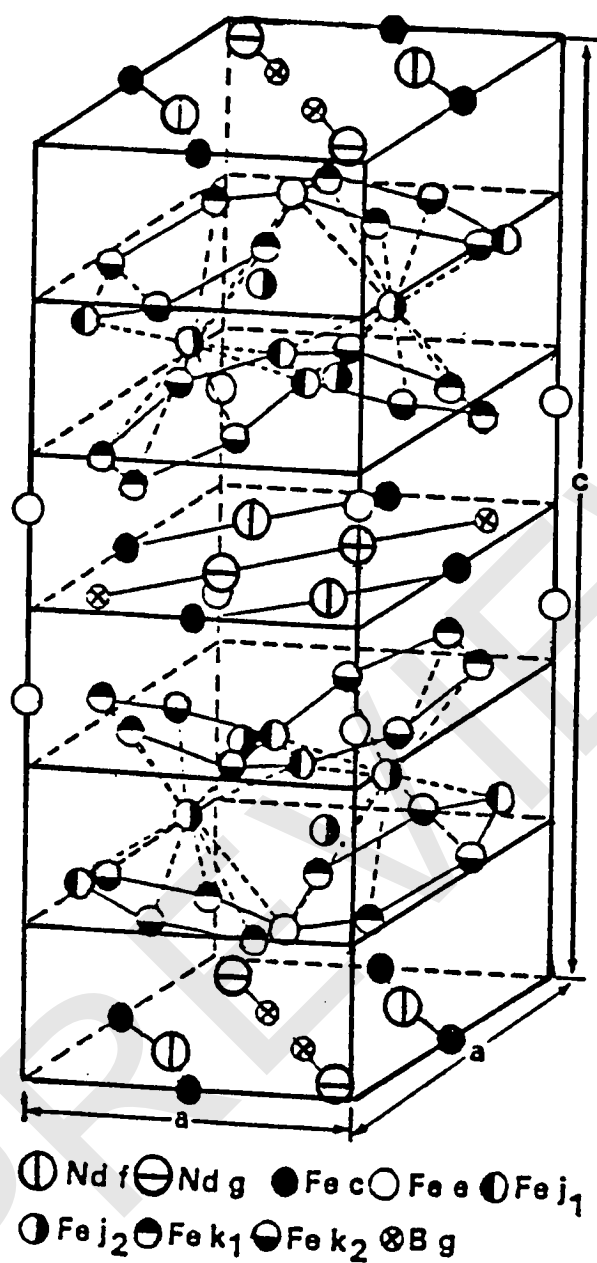


Fig. 3. Crystal structure of $\text{Nd}_2\text{Fe}_{14}\text{B}$. Taken from Ref. 19.